J Mater Sci: Mater Electron (2017) 28:12273–12281
DOI 10.1007/s10854-017-7044-x

Photoluminescence and photocatalytic properties of Ag/AgCl synthesized by sonochemistry: statistical experimental design

N. F. Andrade Neto[1] · L. M. P. Garcia[2] · E. Longo[2] · M. S. Li[3] · C. A. Paskocimas[1] · M. R. D. Bomio[1] · F. V. Motta[1]

Received: 27 January 2017 / Accepted: 28 April 2017 / Published online: 3 May 2017

Abstract Silver chloride (AgCl) particles were produced by sonochemistry synthesis. The effect of the variables such as the time of synthesis, amount of surfactant and reagent in the photocatalytic property of AgCl have were all investigated. AgCl particles became well known for their high photocatalytic activity and their plasmonic properties because of the metallic silver on their surface. In this study, AgCl particles were prepared with sodium chloride (NaCl), polyvinylpyrrolidone and silver nitrate ($AgNO_3$), using a full 2^3 factorial design and three central points, resulting in 11 experiments. The synthesis was carried out using ultrasonic tip at time intervals of 5, 20 and 35 min. It was used X-ray diffraction, scanning electron microscopy with field emission (SEM-FEG), UV–Vis degradation test and photoluminescence to characterize the particles. The experimental design not only used variables present in the photocatalytic ability of the particles, but also provided a mathematical model. The (ANOVA) analysis of variance was used to confirm this model. Thus the values predicted could be observed. It is provided a response surface that characterizes the optimization zone of the photocatalytic activity of the AgCl particles to better visualize the information about its effects.

✉ N. F. Andrade Neto
nfandraden@gmail.com

[1] LSQM, DEMAT, UFRN, Av. Sen. Salgado Filho, 3000, Natal, RN CEP 59072-970, Brazil

[2] LIEC, DQ, UFSCar, Via Washington Luiz, km 235, São Carlos, SP CEP 13565-905, Brazil

[3] IFSC, USP, Av. Trabalhador São Carlense, 400, São Carlos, SP CEP 13566-590, Brazil

1 Introduction

Particulates of silver have had great attention in the technological area in the last decades, some indication of their vast potential have been witnessed in various fields such as catalysis [1], fuel cells [2], lithium-ion batteries [3] etc. In the semiconductor photocatalytic process, under light irradiation, an electron is excited from the valence band to the conduction band and forms holes in valence band which interact wih H_2O or OH^- adsorbed on the surface of the catalyst to generate hydroxyl radical ($OH^•$), or the electron in the conduction band interacts with adsorbed O_2 to yield O_2^- [4]. Metallic particles, especially noble metals particles, usually exhibit high electrocatalytic activities towards the target compounds. Among all the nanomaterials, nanoparticles of silver exhibit catalytic activity for the reduction of H_2O_2 [5, 6].Welch et al. proved that the reduction of H_2O_2 was easier due to the modification of the glassy-carbon electrodes with nanoparticles of silver [5]. These radicals are responsible for the degradation of dye molecules. In general, the photocatalytic efficiency of metal is minimized by the recombination of electron–hole pairs in the bulk of the material. Silver nanoparticles are increasingly known for their high photocatalytic activity due to the metallic particles on their surface (hybrid photocatalysts), which cause a plasmonic effect, leading to a reduction of the electron/hole recombination reaction [1, 7].

Recently, hybrid nanophotocatalysts with metal particles on their surface, acting to produce surface plasmon resonance, have gained great importance in the study of the decomposition of organic pollutants in visible radiation [8–10]. Noble metals on the nanoscale, such as gold and silver, stand out in this property due to their low level of Fermi [11]. Therefore, nanoparticles can be used to absorb visible light and develop new plasmon resonance centers.

The literature [8, 11–14] reported that Ag nanoparticles deposited on a semiconductor enables the generation of electron–hole pairs, which consequently improves the photocatalytic activity to purify applications under the sunlight or visible light irradiation. For example, Au (or Ag) doped with TiO_2 [15], WO_3 [16], ZnO [17], AgX (X = Cl, Br, I) [18], as well as other semiconductors with a large bandgap [19]. AgCl nanocubes were prepared via a reverse micelle method [20]. These results showed how efficiently photocatalysts can drive degradation of organics under sunlight. Nanoparticles of Ag/AgCl, which are AgCl nanoparticles with silver metal deposited on their surface, exhibit strong absorption in the ultraviolet spectral region and low absorption in the visible region due to their band-gap 3.25 eV [20–23].

Huang et al. [24] synthesized particles Ag/AgCl through ion exchange reaction, followed by a reduction using photoinduction in the presence of methyl orange. Sun et al. [25] reported a thermal polyol synthesis in several steps with good photocatalytic property in visible light with methylene blue. However, these synthesis routes usually require few steps and elevated temperatures, moreover they are difficult to control in the particle morphology. Strzalka and Pikus [14] synthesized AgCl nanoparticles to impregnate the mesoporous silica, where the process is divided into two steps, carrying out the reduction of silver ions from the silver nitrate and then mixing them with the mesoporous silica. This synthesis requires a subsequent calcination in the sonochemical process at 550 °C.

In order to eliminate these problems, the ultrasonic synthetic method is extensively studied because it does not usually need high temperatures and various steps during its synthesis, besides that, it is a kind of green synthesis [8, 11–13]. The ultrasound irradiation is known to accelerate chemical reactions [26, 27]. Israr et al. [33] synthesized porous particles of Cu-BTC by irradiating ultrasound between 20 and 120 min at room temperature. It happens primarily due to acoustic cavitation, which is the formation, growth and collapse of bubbles formed by the propagation of pressure waves in the liquid [28–30]. The collapse of the bubbles generates high temperatures and pressures in nanoseconds, accompanied by sonoluminescence and mechanical effects [26, 31, 32]. Thus, the yield obtained with ultrasound reactions is superior to that one obtained under the same conditions using more traditional synthesis procedures, such as sol–gel and Pechini [12, 33, 34].

The methodology of the experimental design coupled with the response surface analysis is a statistical tool that provides reliable information to the process, which minimizes the empiricism that involves trial and error techniques [13, 35, 36]. In addition, the response surface methodology allows a simultaneous investigation of the variables in the chemical synthesis processes such as temperature, time, and concentration, among others. Jung et al. [13] using response surfaces to optimize the electrical activity used it for the degradation of sewage waste.

This study used a full factorial design associated to a response surface analysis to investigate the influence of variables (synthesis time, amount of NaCl and amount of PVP) in the synthesis of AgCl by sonochemistry. Furthermore, the photoluminescence and photocatalytic properties of these samples were investigated. The correlation between the properties and variables of the process was discussed.

2 Materials and methods

2.1 Synthesis Ag/AgCl

The Ag/AgCl powders were obtained using the sonochemical method at 20 kHz frequency. It was added ethylene glycol (Synth, 99,0%) for this synthesis. Polyvinylpyrrolidone (Alfa Aesar, 99,0%), sodium chloride (Dinâmica LTDA, 99,0%) and, silver nitrate (Synth, 99%), were dissolved in 80 mL of distilled water at constant stirring. The amount of AgNO3 was kept constant at 5.1 g L^{-1} for all samples. Then, the samples were taken for the ultrasonic probe Branson 102C, at time intervals of 5, 20 and 35 min. At the end of the synthesis, the samples were washed with distilled water and then, centrifuged.

For experimental design, there was a large amount of NaCl and PVP, as well as the synthesis time. Table 1 shows the planning table with real and coded values used for synthesis and planning.

Table 1 Real values and coded the factors used in the factorial design

Sample	Time synthesis (min) (A)	Amount PVP (gL^{-1}) (B)	Amount NaC1 (gL^{-1}) (C)
P1	5 (−1)	0 (−1)	1.5 (−1)
P2	35 (+1)	0 (−1)	1.5 (−1)
P3	5 (−1)	4.5 (+1)	1.5 (−1)
P4	35 (+1)	4.5 (+1)	1.5 (−1)
P5	5 (−1)	0 (−1)	6 (+1)
P6	35 (+1)	0 (−1)	6 (+1)
P7	5 (−1)	4.5 (+1)	6 (+1)
P8	35 (+1)	4.5 (+1)	6 (+1)
P9	20 (0)	2.25 (0)	3.75 (0)
P10	20 (0)	2.25 (0)	3.75 (0)
P11	20 (0)	2.25 (0)	3.75 (0)

2.2 Characterization

The phase composition of AgCl was investigated in a Shimadzu (XRD-6000) diffractometer using CuKa radiation (0,15418 Å). A scanning electron microscope (SEM) was used to observe its morphology. The photocatalytic properties of the samples were tested (as a catalyst agent) for the degradation of methylene blue (MB) dye with a molecular formula [$C_{16}H_{18}ClN_3S$] (99.5% purity, Mallinckrodt) in an aqueous solution under UV-light illumination. The sample was placed in a cylindrical quartz reactor, containing 50 ml of methylene blue dye solution (concentration 1×10^{-5} mol L^{-1}). Then, a cylindrical quartz reactor was placed into a photo-reactor at controlled temperature (25 °C) and, illuminated by six UVC lamps (TUV Philips, 15 W, with maximum intensity of 254 nm = 4.9 eV). In 30-s intervals, the 3 mL aliquot of the dye solution was taken and analyzed by its variations of the maximum absorption band of MB dye solutions by UV–vis absorbance spectra measurements using a Shimadzu (model UV-2600) spectrophotometer.

3 Results and discussion

XRD was used to determine the crystal structure and purity of the material synthesized via sonochemical. Figure 1 shows the XRD patterns regarding the samples of the experimental design.

All the diffraction peaks present in XRD patterns could be indexed to the cubic lattice [space group *Fm-3m* (225)] related to the AgCl phase (JCPDS Card No. 31-1238).

According the XRD patterns (Fig. 1), the AgCl powders were crystalline and structurally ordered at long range. These results show that the sonochemistry method promoted the complete crystallization of the AgCl sample at low temperatures and reduced the processing time. No secondary phases were detected.

These factors were calculated for the 11 samples and the experiment is shown in Table 2. It is clear in the table that the values found for the experimental samples are very close to the values indicated in the crystallographic letter. The lattice parameters *a* were calculated using the least-square refinement from the UnitCell-97 Maud program. Chen et al. [8] synthesized nanoparticles AgCl through sonochemical without subsequent calcination and obtained a similar crystal structure.

Figure 2 shows the variation of the methylene blue concentration over the time under UV light degradation. Wang and co workers [6] showed that AgCl particles have a large energy absorption only in the spectral region of the ultraviolet, whereas the Ag/AgCl particles exhibit high absorption throughout the visible region, and this

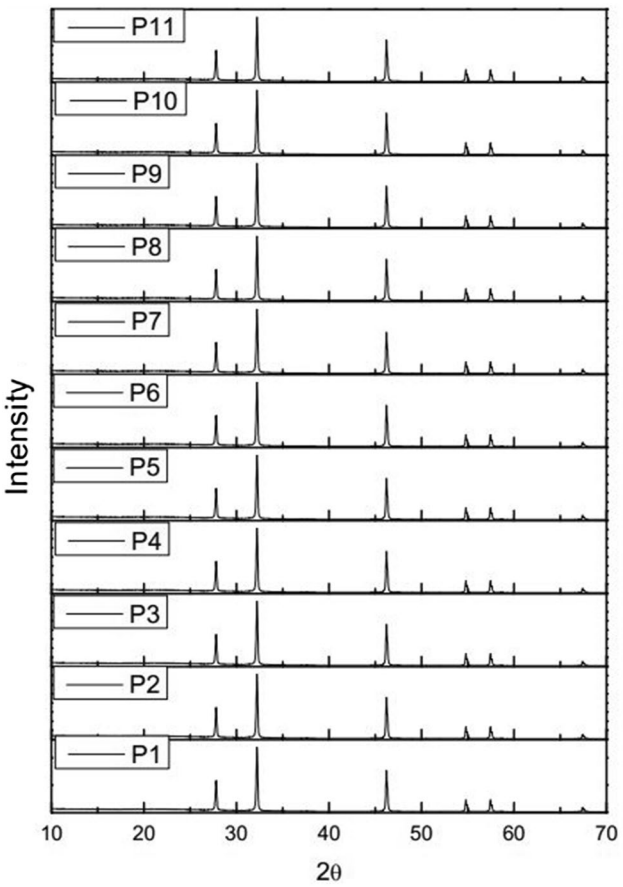

Fig. 1 XRD patterns of AgCl particles obtained by sonochemical method

Table 2 Lattice constants (a, Å), cell volumes (V, $Å^3$) and the average crystallite size (Dcrys, nm) of the cubic structure of AgCl powders prepared by the sonochemistry method

Sample	Dcrys (nm)	*a* (Å)	V ($Å^3$)
P1	61.5391	5.558515	171.741933
P2	63.4462	5.561145	171.985826
P3	62.9115	5.363838	154.321855
P4	62.9116	5.562715	172.131530
P5	66.1372	5.544265	170.424465
P6	70.8084	5.558421	171.733220
P7	65.0978	5.555868	171.496696
P8	64.2707	5.557527	171.650370
P9	70.0999	5.54207	170.222130
P10	70.1243	5.541644	170.182880
P11	70.2919	5.541901	170.206558
JCPDS card No. 31–1238	–	5.5490	170.861484

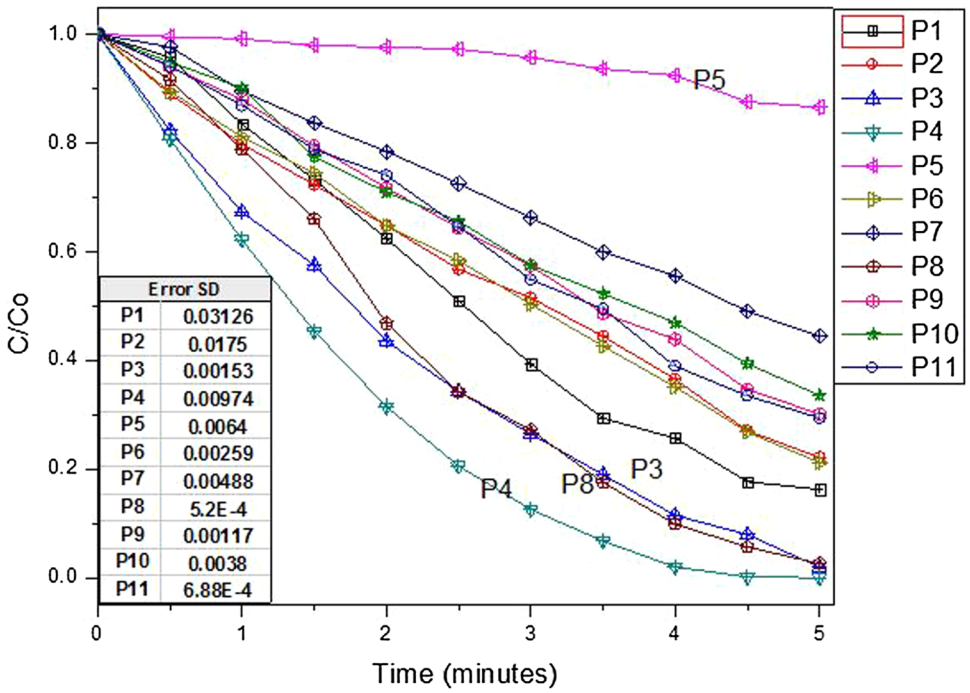

Fig. 2 Methylene blue degradation under UV radiation for samples of the experimental design. The results are means of duplicates

fact is associated with the silver particles deposited on the surface of the particles.

Particles of methylene blue can be effectively decomposed under ultraviolet light, with the aid of Ag/AgCl particles, as shown in Fig. 2. The P4 sample showed a higher rate of decomposition, which takes about 4 min for the complete degradation of the solution. Subsequently, the samples P8 and P3 had satisfactory results for the time of 5 min, in which almost the total degradation of the solution occurs. In a large-scale production, considering the difference in the synthesis time of P3 and P4 compounds, P3 sample is more advantageous because it is synthesized in 5 min while P4 is synthesized in 35 min. Sample P5 showed the worst results, where an interruption of 5 min in the test, reduced only about 14% of the methylene blue solution.

The addition of PVP is essential in the formation of the particulate, since it acts to hold the spacing of the particles, avoiding their agglomeration. Fernandes et al. [38] noted in nano-hydroxyapatite particles that PVP forms a sort of ball with the material, thus hindering the growth and agglomeration of the particles. A greater amount of NaCl causes a decrease in the Ag/Cl ratio and the reduction of silver ions also decreases the photocatalytic activity. Chen et al. [8] showed that the concentration of silver ions on the particle increases its degradation rate.

Figure 3 shows the images obtained by SEM, for the particles in the UV degradation highlighted which is used to observe their morphology thereof.

Liu et al. [34] reported that a high PL intensity implies a high recombination of electron–holes photogenerated with incident radiation, thus generating few electron–hole pairs to act in the oxidation and reduction reactions, thereby reducing the photocatalytic activity of the material. It can be seen by comparing Figs. 2 and 4 that P4 sample, which better presents the photocatalysis result, has the lowest photoluminescence intensity. Whereas P5 sample, which has the highest intensity in photocatalysis, presents a worse performance in the methylene blue photocatalysis.

Chen et al. [39] observed that silver particles have broad absorption bands centered at 450 nm before undergoing UV irradiation. As shown in Fig. 4a, the absorption peaks coincide with 450 nm, so that the material may also absorb energy in the visible range.

The various types of defects in the structure promote different distributions at intermediate levels between the valence band and the conduction band [40]. Therefore, these changes in the electronic structure affects the optical properties of the material. Figure 5 shows the absorption spectra in the UV–visible region of P4 and P5 samples. The optical gap was obtained by extrapolating the linear region of the curve according to the method of Tauc [41]. The gap values for P4 and P5 samples were 3.20 and 2.93 eV, respectively. These values are close to that reported in the literature, which is 3.25 eV [20–23]. The decrease of the band gap is associated with an increase in the structural defects existing in the material lattice [42].

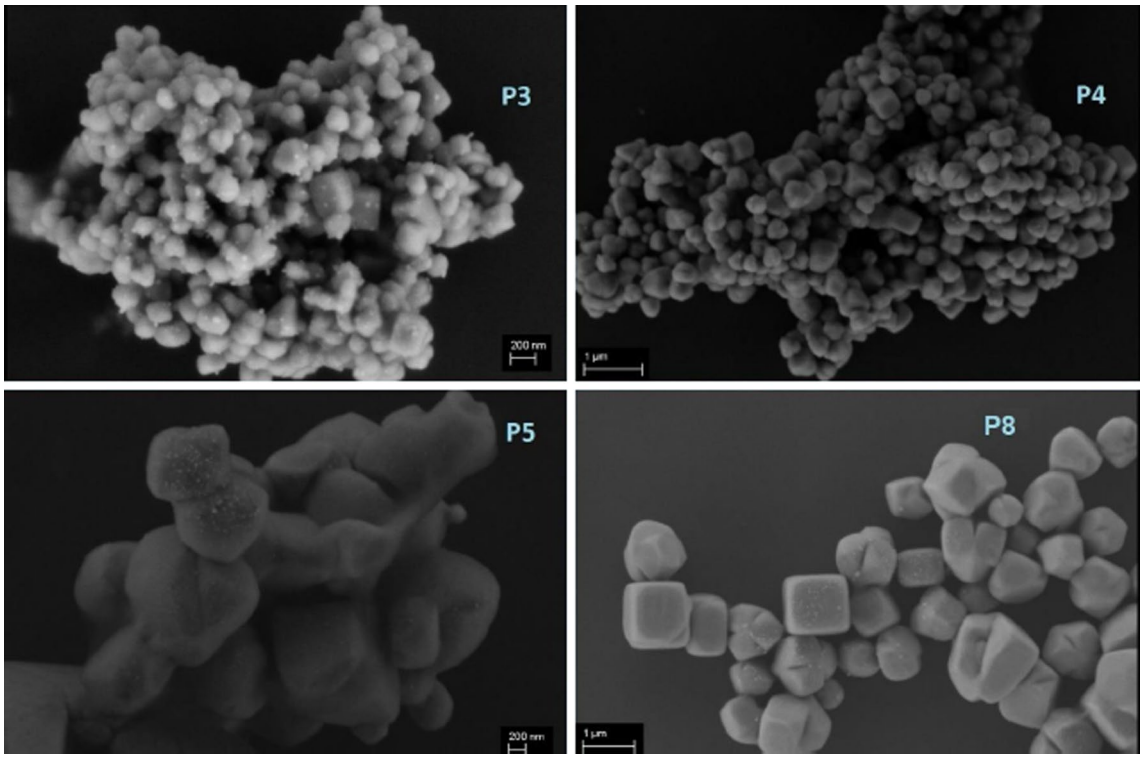

Fig. 3 FE-SEM images of AgCl powders prepared using sonochemistry method

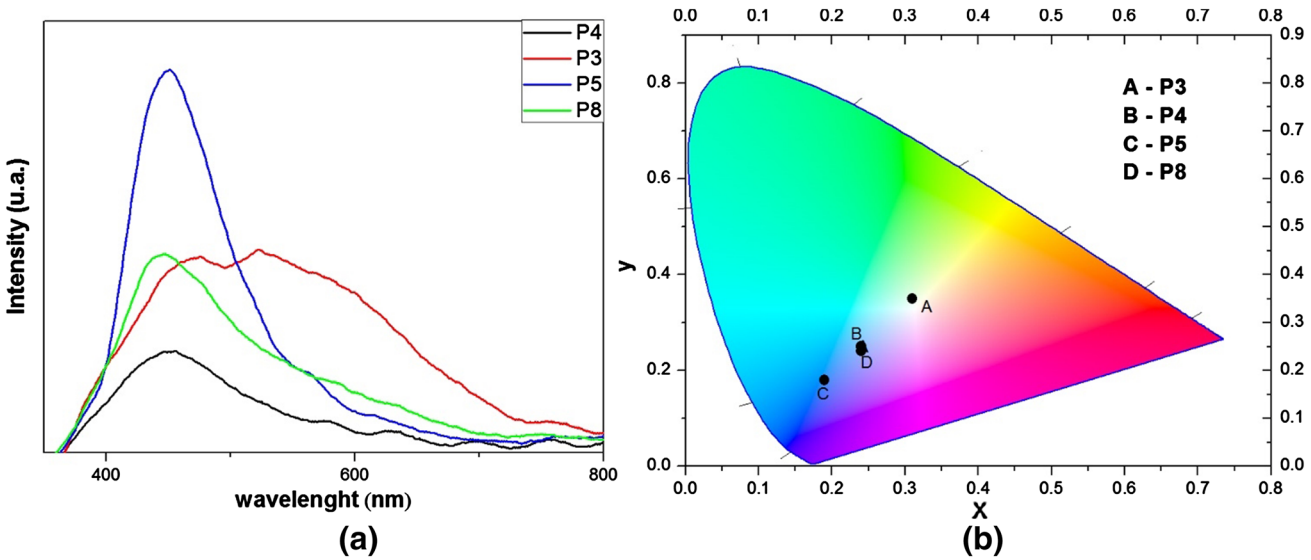

Fig. 4 **a** Photoluminescence spectra and **b** CIE, for the samples highlighted in the photocatalysis

3.1 Experimental design

The determination of the empirical model using Statistica Software was based on the degradation time values obtained within four and a half minutes (270 s) of UV aging, as shown in Table 1, with three midpoints. The model obtained for the percentage of degradation, in terms of coded values is:

The results for the regression are shown in Table 3. It was applied the analysis of variance to assess the relevance and adequacy of the model, and the effects of the individual terms and their significant interactions in the chosen

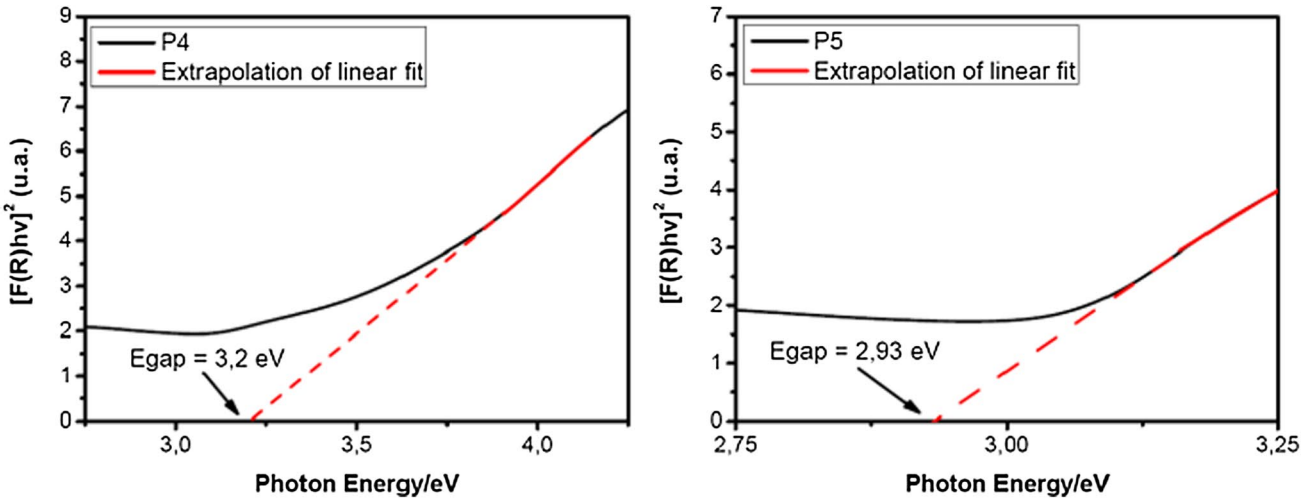

Fig. 5 Absorption spectra in the UV–visible region extrapolating the linear region of the curve according to the method of Tauc for samples P4 and P5

Table 3 Results for parameters estimation for the model obtained

Terms	Coefficient	Standard-error	t(2)	p
Constant	0.7008	0.0095	74.1516	0.00018
A	0.1282	0.0222	11.5700	0.00739
B	0.1203	0.0222	10.8614	0.00837
C	−0.1453	0.0222	−13.1122	0.00577
A.C	0.1321	0.0222	11.9190	0.00697
A.B.C	−0.0432	0.0222	−3.8964	0.06000

responses. Table 4 shows that all terms in the model were significant at the 95% confidence ($p < 0.05$).The interaction effect of the three variables was taken into account for the model construction due to its proximity to the confidence level. Figure 6 shows a graph of predicted and observed values, which is also used to validate the model obtained. For this chart, the closer the points are from the drawn line, the more reliable the model is.

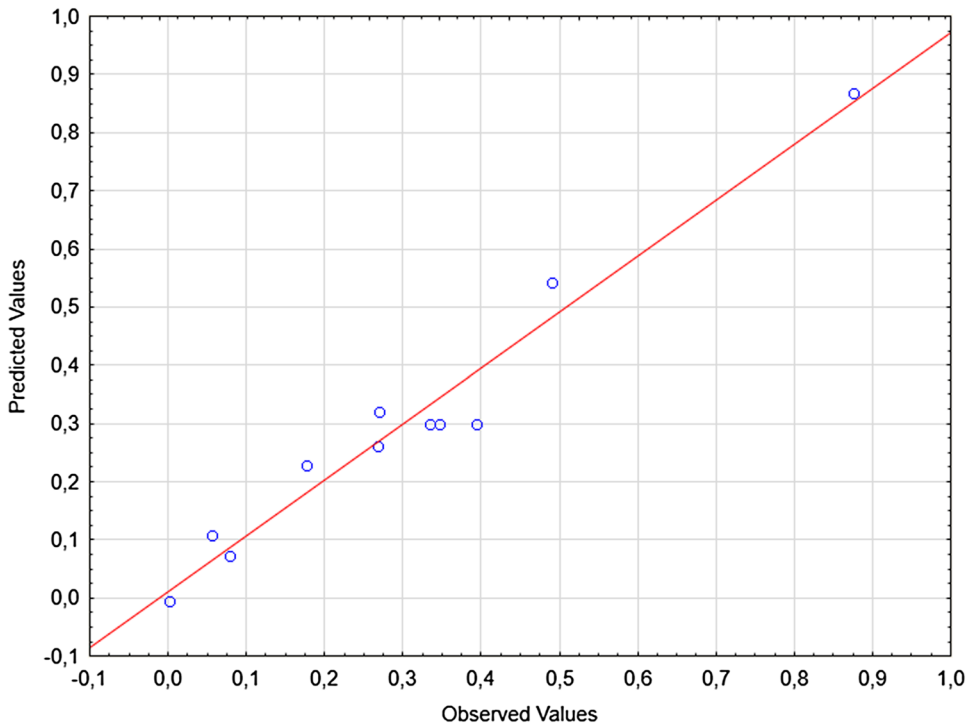

Fig. 6 Predicted values and observed values

Table 4 ANOVA results of experimental design for the degradation yield

	SS	DF	MS	F
Regression	0.5710	5	0.1141	24.95
Residual	0.0230	5	0.004575	
Lack of fit	0.0209	3		
Pure error	0.001965	2		
Total	0.5937	10		

Another way to analyze the reliability of the model is the F value shown in Table 4. The value obtained in this model was 24.95 and for analysis of reliability, this value shall be compared to the F-distribution provided by Snedecor to 5%, which is 5.05. For the model to be considered significant, the F value obtained must be at least three times greater than the Snedecor distribution. For this mode, the F value achieved was approximately five times higher.

Through this model it is possible to determine the effect of variables regarding the degradation of the methylene blue solution. Through the surfaces shown in Fig. 7 and the model obtained, it is concluded that the increase of the synthesis time and the amount of PVP when analyzed individually, act positively on the degradation capacity of the material, while the NaCl concentration acts negatively on the degradability of the same. When the effect of NaCl in the interaction with the synthesis time is taken into consideration, this increase results in an increase in the solution degradability. The analysis of the effects of the variables via response surface is the simplest and fastest way to be performed. They show through colors and tilt the best levels to be used to obtain the highest yield of degradation [13, 43]. On these surfaces, the optimized values are always in the darkest parts.

4 Conclusions

Even with the change in the composition of the particles, all of them presented the same crystalline phase described by the JCPDS card in 31-1238, and showed metallic silver

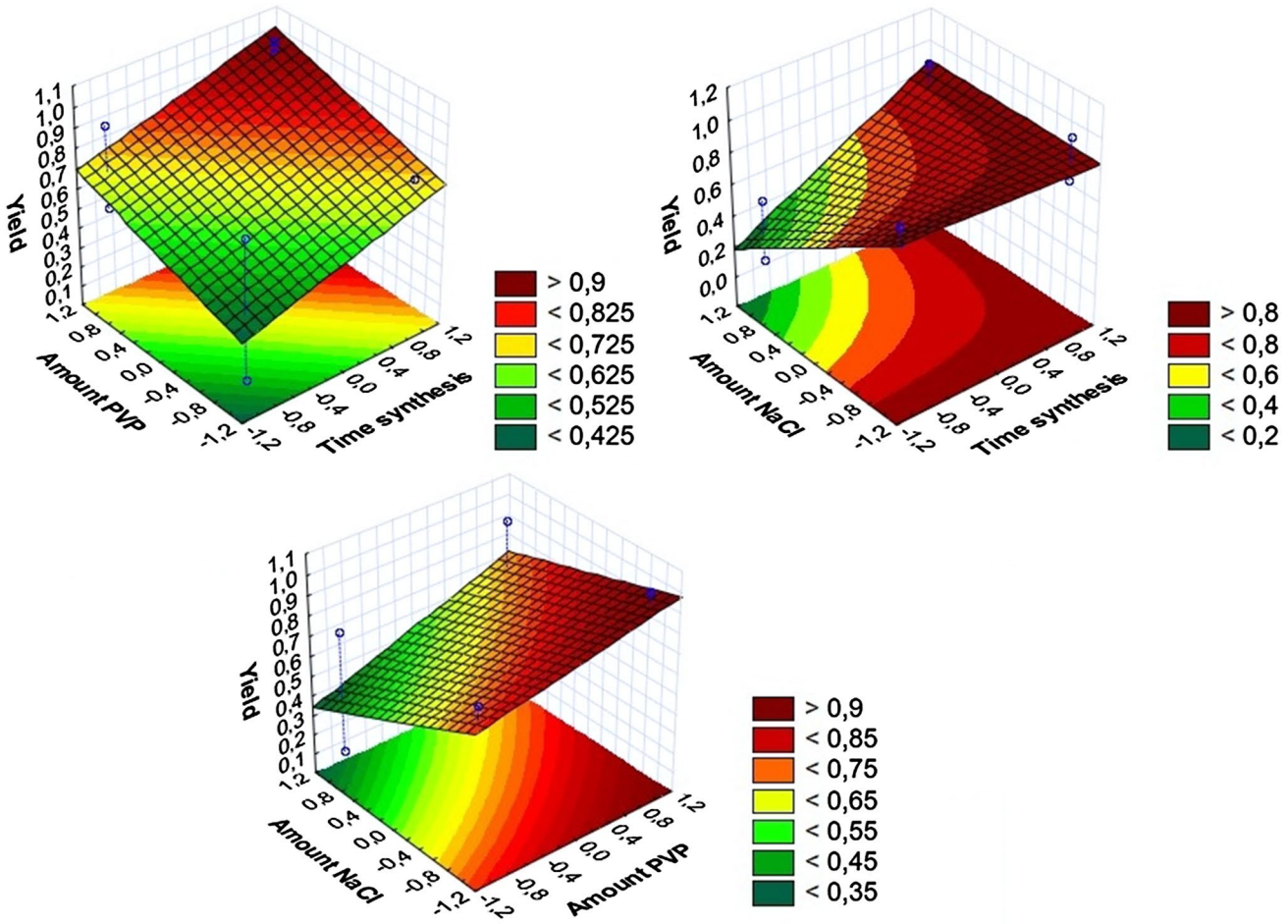

Fig. 7 RSM for the model obtained

deposited on their surface. It was noted that the particle size showed no direct influence in the photocatalytic activity of the particles. In short, the particles have a cubic morphology, which was expected for the sonochemical synthesis of the silver chloride. Through the response surface, it was determined that the increase in the synthesis time and in the amount of PVP showed positive influence on the catalytic activity, while increasing the amount of NaCl showed a negative influence on it. Samples with the best photocatalytic properties performed worst in photoluminescent properties. According to the results of photoluminescence, P4, P5 and P8 samples showed emission in blue, while P3 sample showed emission in green.

Acknowledgements The authors thank the financial support of the Brazilian research financing institutions: CAPES, CNPq N° 402127/2013-7 and FAPESP 2013/07296-2.

References

1. M.L. Yola, T. Eren, N. Atar, S. Wang, Adsorptive and photocatalytic removal of reactive dyes by silver nanoparticle-colemanite ore waste. Chem. Eng. J. **242**, 333–340 (2014)
2. M.L. Yola, T. Eren, N. Atar, H. Saral, I, Ermis; functionalized Fe_3O_4/graphene oxide nanocomposites with hairpin aptamers fotr the separation and preconcentration of trace Pb^{2+} from biological samples prior to determination by ICP MS. Electroanalysis **28**, 570–579 (2016)
3. N. Atar, T. Eren, M.L. Yola, H. Genrengi, S. Wang, Fe/Ag nanoparticles decorated reduced graphene oxide as ultrahigh capacity anode material for lithium-ion battery. Ionics **21**, 3185–3192 (2015)
4. J.H. Sun, S.Y. Dong, Y.K. Wang, Preparation and photocatalytic property of a novel dumbbell-shaped ZnO microcrystal photocatalyst. J. Hazard. Mater. **172**, 1520–1526 (2009)
5. C.M. Welch, C.E. Banks, A.O. Simm, R.G. Comptom, Silver nanoparticle assemblies supported on glassy-carbon electrodes for the electro-analytical detection of hydrogen peroxide. Anal. Bioanal. Chem. **382**, 12 (2005)
6. K. Cui, Y.H. Song, Y. Yao, Z.Z. Huang, L. Wang, A novel hydrogen peroxide sensor based on Ag nanoparticles electrodeposited on DNA-networks modified glassy carbono electrode. Electrochem. Commun. **10**, 663 (2008)
7. J.F. Guo, B. Ma, A. Yin, K. Fan, W.L. Dai, Photodegradation of rhodamine B and 4-chlorophenol using plasmonic photocatalyst of Ag–AgI/Fe_3O_4@SiO_2 magnetic nanoparticle under visible light irradiation. Appl. Catal. B **101**, 580–586 (2011)
8. D. Chen, S.H. Yoo, Q. Huang, G Ali, S.O. Cho, Sonochemical synthesis of Ag/AgCl nanocubes and their efficient visible-light-driven photocatalytic performance. Chem. Eur. J. **28**, 5192–5200 (2012)
9. I.L. Sayed, V.V. Thakhur, M.D. Nikalje, G.K. Dewkar, S.P. Kotkar, Asymmetric synthesis of aryloxypropanolamines via OsO 4-catalyzed asymmetric dihydroxylation. Tetrahedron **61**, 2831–2838 (2005)
10. Q.J. Xiang, J.G. Yu, B. Cheng, Microwave-assisted hydrothermal synthesis of cube-like Ag-Ag2MoO4 with visible-light photocatalytic activity. Chem. Asian J. **5**, 1466–1474 (2010)
11. W. Dai, H. Xu, L. Yang, X. Luo, X. Tu, Ultrasonic-assisted facile synthesis of plasmonic Ag@AgCl cuboids with high visible light photocatalytic performance for Rhodamine B degradation. React. Kinet. Mech. Catal. **115**, 773–786 (2015)
12. J.P.S. Fernandes, B.S. Carvalho, C.V. Luchez, M.J. Politi, C.A. Brandt, Optimization of the ultrasound-assisted synthesis of allyl 1-naphthyl ether using response surface methodology. Ultrason. Sonochem. **18**, 489–493 (2011)
13. K.W. Jung, M.J. Hwang, M.J. Cha, K.H. Ahn, Application and optimization of electric field-assisted ultrasonication for disintegration of waste activated sludge using response surface methodology with a Box-Behnken design. Ultrason. Sonochem. **22**, 437–445 (2015)
14. M.Z. Strzalka, S. Pikus, Synthesis of photoactive AgCl/SBA-15 by conversion of silver nanoparticles into stable AgCl nanoparticles. Appl. Surf. Sci. **265**, 904–911 (2013)
15. N. Barsan, U. Waimer; Conduction model of metal oxide gas sensors. J. Electroceramic, **7**, 143–167, (2001)
16. A. Tanaka, K. Hashimoto, H. Kominami, Plasmonic Au/Pd nanoparticles supported on a basic metal–organic framework: synergic boosting of H_2 production from formic acid. J. Am. Chem. Soc. **136**, 586–589 (2014)
17. Y. Chen, D. Zeng, K. Zhang, A. Lu, L. Wang, Au–ZnO hybrid nanoflowers, nanomultipods and nanopyramids: one-pot reaction synthesis and photocatalytic properties. Nanoscale **6**, 874–881 (2014)
18. X. Ma, Y. Dai, M. Guo, B. Huang, The role of effective mass of carrier in the photocatalytic behavior of silver halide-based Ag@AgX(X = Cl, Br, I): a theoretical study, Chem. Phys. Chem. **13**, 2304–2309 (2012)
19. A. Tanaka, K. Hashimoto, H. Kominami, Preparation of Au/CeO_2 exhibiting strong surface plasmon resonance effective for selective or chemoselective oxidation of alcohols to aldehydes or ketones in aqueous suspensions under irradiation by green light. J. Am. Chem. Soc. **134**, 14526–14533 (2012)
20. C. An, R. Wang, S. Wang, X, Zhang; Converting AgCl nanocubes to sunlight-driven plasmonic AgCl: Ag nanophotocatalyst with high activity and durability. J. Mater. Chem. **21**, 11532–11536 (2011)
21. C. An, X. Ming, J. Wang, Construction of magnetic visible-light-driven plasmonic Fe_3O_4-SiO_2-AgCl: Ag nanophotocatalyst. J. Mater. Chem. **22**, 5171–5176 (2012)
22. P. Wang, T.F. Xie, H.Y. Li, L. Peng, Y. Zhang, Synthesis and plasmon-induced charge-transfer properties of monodisperse gold-doped titania microspheres. Chem. Eur. J. **15**, 4366–4372 (2009)
23. L. Du, A. Furube, H. Yamamoto, K. Hara, R. Katoh, M. Tachiya, Plasmon-induced charge separation and recombination dynamics in gold–TiO_2 nanoparticle systems: dependence on TiO_2 particle size. J. Phys. Chem. C **113**, 6454–6462 (2009)
24. B. Huang, P. Wang, X. Quin, X. Zhang, Y. Dai, Ag/AgCl: a highly efficient and stable photocatalyst active under visible light. Angew. Chem, Int. Ed. **47**, 7931–7933 (2008)
25. C. An, S. Peng, Y. Sun, Facile synthesis of sunlight-driven AgCl:Ag plasmonic nanophotocatalyst. Adv. Mater. **22**, 2570–2574 (2010)
26. G. Cravottoa, P. Cintas, Forcing and controlling chemical reactions with ultrasound. Angew. Chem. Int. Ed. **46**, 5476–5478 (2007)
27. C.A. Brandt, A.C. Da Silva, C.G. Pancote, C.L. Brito, Efficient synthesis method for β-enamino esteers using ultrasound. Synthesis **2004**, 1557–1559 (2004)
28. J. Jiang, Z.L. Zhang, Rapid microwave-assisted nonaqueous synthesis and growth mechanism of AgCl/Ag and its daylight-driven plasmonic photocatalysis. Chem. Eur. J. **17**, 3710–3717 (2011)
29. S.M. Zhu, H.A. Zhou, M. Hibino, I. Honma, M, Ichihara; Synthesis of MnO_2 nanoparticles confined in ordered mesoporous

carbon using a sonochemical method. Adv. Funct. Mater. **15**, 381–386 (2005)
30. J.H. Bang, K.S. Suslick, Applications of ultrasound to the synthesis of nanostructured materials. Adv. Mater. **22**, 1039–1059 (2010)
31. J. Kim, C. Park, T.H. Kim, M. Lee, Effects of various pretreatments for enhanced anaerobic digestion with waste activated sludge. Biosci. Bioeng. **95**, 271–275 (2003)
32. J. Han, P. Fang, W. Jiang, R. Guo, Ag-Nanoparticle-loaded mesoporous silica: spontaneous formation of Ag nanoparticles and mesoporous silica SBA-15 by a one-pot strategy and their catalytic applications. Langmuir **28**, 4768–4775 (2012)
33. F. Israr, D.K. Kim, Y. Kim, S.J. Oh, K.C. Ng, Synthesis of porous Cu-BTC with ultrasonic treatment: effects of ultrasonic power and solvent condition. Ultrason. Sonochem. **29**, 186–193 (2016)
34. X. Liu, W. Huang, G. Huang, F. Fu, H. Cheng, W. Guo, Synthesis of bilayer ZnO nanowire arrays: morphology evolution, optical properties and photocatalytic performance. Ceram. Int. **41**, 11710–11718 (2015)
35. X. Song, Y. Gao, F. Yuan, Optimization of antioxidant peptide production from goat placenta powder using RSM. Food Sci. Technol. **33**, 237–241 (2008)
36. K.W. Jung, D.H. Kim, H.W. Kim, Optimization of combined (acid + thermal) pretreatment for fermentative hydrogen production from Laminaria japonica using response surface methodology (RSM). Int. J. Hydrog. Energy **36**, 9626–9631 (2011)
37. R. Wang, C. An, S. Wang, Z. Zhang, Converting AgCl nanocubes to sunlight-driven plasmonic AgCl: Ag nanophotocatalyst with high activity and durability. J. Mater. Chem. **21**, 11532 (2011)
38. T.J. Fernandes, PVP Síntese de hidroxiapatita nanométrica com,: sintetização e adsorção de albumina bovina. Dissertação de Mestrado apresentada ao Curso de Mestrado em Engenharia dos Materiais do Instituto Militar de Engenharia, Rio de Janeiro, 2011
39. Y. Chen, T. Yang, H. Pan, Y. Yuan, L. Chen, Photoemission mechanism of water-soluble silver nanoclusters: ligand-to-metal–metal charge transfer vs strong coupling between surface plasmon and emitters. Am. Chem. Soc. **136**, 1686–1689 (2014)
40. L.S. Cavalcante, F.M.C. Batista, M.A.P. Almeida, A.C. Rabelo, I.C. Nogueira, N.C. Batista, J.A. Varela, M.R.M.C. Santos, E. Longo, M. Li., Siu; Structural refinement, growth process, photoluminescence and photocatalytic properties of ($Ba_{1-x}Pr_{2x/3}$) WO_4 crystals synthesized by the coprecipitation method. RSC. Adv. **2**, 6438 (2012)
41. D.L. Wood, J, Tauc; Weak absorption tails in amorphous semiconductors. Phys. Rev. B **5**(8), 3144 (1972)
42. D. Ding, K. Liu, S. He, C. Gao, Boosting up the low catalytic activity of silver for H_2 production on Ag/TiO_2 photocatalyst: thiocyanate as a selective modifier. Nano Lett. **14**, 6731–6736 (2014)
43. J.P.S.F. Fernandes, B.S. Carvalho, C.V. Luchez, M.J. Politi, C.A. Brandt, Optimization of the ultrasound-assisted synthesis of allyl 1-naphthyl ether using response surface methodology. Ultrason. Sonochem. **18**, 489–493 (2011)